Semibatch RAFT Polymerization for Producing ST/BA Copolymers with Controlled Gradient Composition Profiles

Xiaoying Sun
The State Key Laboratory of Chemical Engineering, Dept. of Chemical and Biochemical Engineering, Zhejiang University, Hangzhou 310017, People's Republic of China

School of Biological and Chemical Engineering, Zhejiang University of Science and Technology, Hangzhou 310012, People's Republic of China

Yingwu Luo, Rui Wang, and Bo-Geng Li
The State Key Laboratory of Chemical Engineering, Dept. of Chemical and Biochemical Engineering, Zhejiang University, Hangzhou 310017, People's Republic of China

Shiping Zhu
Dept. of Chemical Engineering, McMaster University, Hamilton, Ontario, Canada L8S 4L7

DOI 10.1002/aic.11446
Published online February 19, 2008 in Wiley InterScience (www.interscience.wiley.com).

With controlled/living radical copolymerization, the composition profile along polymer chains becomes a tunable parameter in preparing copolymer products for novel materials properties. In this work, a novel series of styrene/butyl acrylate (St/BA) copolymers with precisely designed composition profiles (uniform, linear gradient, tanh gradient, and triblock with a linear gradient mid-block) were produced using a semibatch reversible addition-fragmentation chain transfer copolymerization mediated by benzyl dithioisobutyrate. The comonomer feeding rate was programmed based on a kinetic model with the targeted composition profile as an objective functions. The experimental composition and molecular weight profiles agreed very well with the model predictions. The polymer molecular weight distributions were narrow with polydispersity index values about 1.3. The amount of dead chains was controlled below 10%. The glass transition behaviors of the St/BA copolymers were evaluated and their T_g values were found to be in an order of uniform < linear gradient < tanh gradient < triblock with 10°C for uniform and 140°C for triblock copolymers. © 2008 American Institute of Chemical Engineers *AIChE J,* 54: 1073–1087, 2008
Keywords: semibatch reactor system, computer-aided design, RAFT polymerization, copolymer composition, gradient copolymer, block copolymer, polymerization kinetics

Introduction

Over half of the total polymeric materials are produced by free radical polymerization processes. In the conventional free radical polymerization, polymer chains are continuously

Correspondence concerning this article should be addressed to Y. Luo at yingwu.luo@zju.edu.cn, B.-G. Li at bgli@zju.edu.cn, or S. Zhu at zhuship@mcmaster.ca

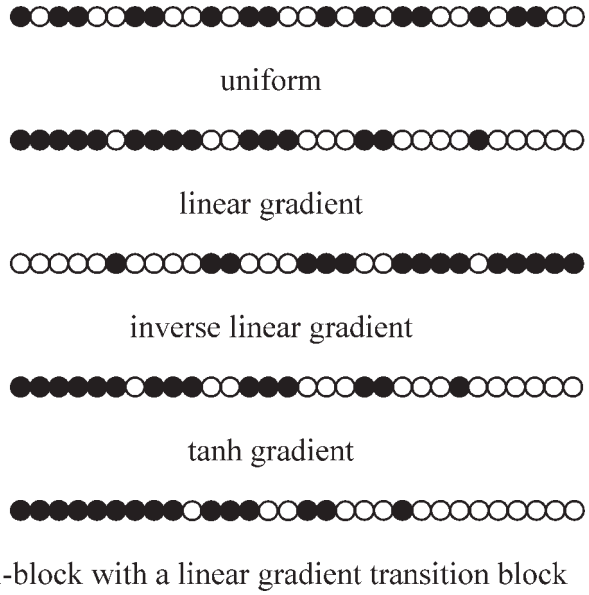

Scheme 1. Schematic representation of the CC profiles with uniform, linear gradient, inverse linear gradient, tanh gradient, and triblock with a linear gradient transition mid block.

The open circles denote Monomer 1 (St) and the closed circles denote Monomer 2 (BA).

initiated and terminated. The lifetime of a propagating chain is very short at a level of seconds. Under such a condition, precise control over microstructural properties of individual chains becomes very difficult. The recent advent of controlled/living radical polymerization (CLRP) techniques provides a great opportunity for tackling this problem and makes the control of chain properties no longer a formidable task.[1–3] Several CLRP techniques have recently been established including nitroxide-mediated polymerization (NMP),[4–6] atom transfer radical polymerization (ATRP),[7–9] and reversible addition-fragmentation chain transfer radical polymerization (RAFT).[10–12] CLRP has been extensively exploited for the synthesis of a large variety of polymers with predetermined molecular weight (MW) and narrow molecular weight distribution (MWD), as well as with well-defined block, star, graft, and brush architectures.[13–17]

On the other side, copolymerization is of particular importance in tuning and balancing materials properties of polymer products. Adjusting the type and amount of comonomers allows us to tailor-make the materials properties such as glass transition temperature to meet specific requirements for certain applications. Different from homopolymer products, copolymer composition (CC) and copolymer composition distribution (CCD), as well as MW and MWD, are all the key parameters that determine materials properties of copolymer products.

Controlled/living radical copolymerization (CLRcoP) combines CLRP with copolymerization. It provides great opportunities for producing unprecedented copolymer products with tailor-made chain microstructures and thus materials properties. It is well-known that a batch-wise process of conventional free radical copolymerization produces a copolymer product which is actually a blend of individual polymer chains of various compositions. This is due to a "composition drifting" effect caused by the different reactivity ratios of the comonomers, as well as to the "instantaneous" growth of individual chains (in seconds). In this case, one monomer is consumed faster than the other, and thus the early born chains are in rich of the fast-monomer units and the later born chains contain more slow-monomer units.

In CLRcoP, individual polymer chains are all born in a relatively short period of time at the beginning, but grow slowly and continuously throughout the whole course of polymerization that usually takes hours. All the chains thus have similar compositions but possess a composition profile from one end to the other. Such products are termed "gradient" or "tapered" copolymers.[1] The synthesis of gradient copolymers using batch CLRcoP processes has been well demonstrated.[18–22] However, the obtained copolymer products have as-synthesized gradient compositions determined only by the comonomer reactivity ratios.

Table 1. Elementary Reactions Involved in RAFT Copolymerization

Reaction Type	Scheme
Initiation	$I \xrightarrow{f,k_d} 2P_0^\bullet$
	$P_0^\bullet + M_j \xrightarrow{k_{i,j}} P_{i,j}^\bullet$
Propagation	$P_{r,ij}^\bullet + M_k \xrightarrow{k_{p,ijk}} P_{r+1,jk}^\bullet, \quad r = 1,2,\ldots$
Preequilibrium	$P_{r,ij}^\bullet + TP_0 \xleftrightarrow{k_{a,j}/k_{f,j}} P_{r,ij}\dot{T}P_0 \xleftrightarrow{k_{a,0}/k_{f,0}} P_0^\bullet + TP_{r,ij}$
Coreequilibrium	$P_{r,ij}^\bullet + TP_{s,kl} \xleftrightarrow{k_{a,j}/k_{f,j}} P_{r,ij}\dot{T}P_{s,kl} \xleftrightarrow{k_{a,1}/k_{f,1}} P_{s,kl}^\bullet + TP_{r,ij}$
Termination	$P_{r,ij}^\bullet + P_{s,kl}^\bullet \xrightarrow{k_{tc,jl}} P_{s+r}$
	$P_{r,ij}^\bullet + P_{s,kl}^\bullet \xrightarrow{k_{td,jl}} P_r + P_s$
	$P_{r,ij}^\bullet + P_{s,kl}\dot{T}P_{t,mn} \xrightarrow{k_{ct}} P_{r+s+t}$

Table 2. Definition of Various Chain Moments

Type of Chains	Definition of Moments
Propagating radical	$Y_m^{ij} = \sum_{r=2}^{\infty} r^m [P_{r,ij}^\bullet]$
Dormant	$Z_m^{ij} = \sum_{r=2}^{\infty} r^m [TP_{r,ij}]$
Primary intermediate radical	$T_m^{ij} = \sum_{r=2}^{\infty} r^m [P_{r,ij}\dot{T}P_0]$
Intermediate radical	$X_m^{ij,kl} = \frac{1}{2}\sum_{r=2}^{\infty} r^m \sum_{s=2}^{r-2} [P_{s,ij}\dot{T}P_{r-s,kl}] \quad (i=k, j=l)$
	$X_m^{ij,kl} = \sum_{r=2}^{\infty} r^m \sum_{s=2}^{r-2} [P_{s,ij}\dot{T}P_{r-s,kl}]$ $(i \neq k)$ or $(j \neq l)$
	$X_{m,n}^{ij,kl} = \sum_{r=2}^{\infty}\sum_{s=2}^{\infty} r^m s^n [P_{r,ij}\dot{T}P_{s,kl}]$
Dead	$Q_m = \sum_{r=2}^{\infty} r^m [P_r]$

Table 3. Differential Moment Equations

Zeroth-order moments (i.e. molar conc. of chains)	Propagating radical chains	$\frac{dY_0^{ij}}{dt} = k_{p,ij}[P_{1,i}^{\bullet}][M_j] + \sum_k k_{p,kij}[M_j]Y_0^{kl} - \sum_k k_{p,ijk}[M_k]Y_0^{ij} - k_{a,j}Y_0^{ij}\left([TP_0] + \sum_k\sum_l Z_0^{kl}\right) + \frac{1}{2}k_{f,j}\left(T_0^{ij} + \sum_{k\neq l}\sum_{orl\neq l} X_0^{ij,kl} + 2\sum_{k=i}\sum_{l=j} X_0^{ij,kl}\right) - [k_{tc,0}[P_0^{\bullet}] + \sum_k\sum_l (k_{tc,jl} + k_{td,jl})Y_0^{kl}]Y_0^{ij} - k_{ct}Y_0^{ij}\left([P_0\dot{T}P_0] + \sum_k\sum_l T_0^{kl} + \sum_k\sum_l\sum_m\sum_n X_0^{kl,mn}\right)$
	Dormant chains	$\frac{dZ_0^{ij}}{dt} = \frac{1}{2}\left(k_{f,0}T_0^{ij0} + \sum_k k_{f,k}T_0^{ijk} + \sum_{k\neq i}\sum_{orl\neq j} k_{f,l}X_0^{ij,kl} + 2\sum_{k=i}\sum_{l=j} k_{f,l}X_0^{ij,kl}\right) - \left(k_{a,0}[P_0^{\bullet}] + \sum_k\sum_l k_{a,l}Y_0^{kl}\right)Z_0^{ij}$
	Primary intermediate radical chains	$\frac{dT_0^{ij}}{dt} = k_{a,0}[P_0^{\bullet}]Z_0^{ij} + k_{a,j}\sum[TP_0]Y_0^{ij} - \frac{1}{2}\left(k_{f,0} + k_{f,j}\right)T_0^{ij} - k_{ct}T_0^{ij}\left([P_0^{\bullet}] + \sum_k\sum_l Y_0^{kl}\right)$
	Intermediate radical chains	$\frac{dX_0^{ij,kl}}{dt} = k_{a,j}Y_0^{ij}Z_0^{kl} - k_{f,j}X_0^{ij,kl} - k_{ct}X_0^{ij,kl}\left([P_0^{\bullet}] + \sum_m\sum_n Y_0^{mn}\right)\ (i=k, j=l)$
		$\frac{dX_0^{ij,kl}}{dt} = k_{a,j}Y_0^{ij}Z_0^{kl} + k_{a,l}Y_0^{kl}Z_0^{ij} - \frac{1}{2}\left(k_{f,j} + k_{f,l}\right)X_0^{ij,kl} - k_{ct}X_0^{ij,kl}\left([P_0^{\bullet}] + \sum_m\sum_n Y_0^{mn}\right)$ $(i\neq k)\ \text{ or }\ (j\neq l)$
	Dead chains	$\frac{dQ_0}{dt} = (k_{tc,0} + k_{td,0})[P_0^{\bullet}]\sum_i\sum_j Y_0^{ij} + \frac{1}{2}\sum_i\sum_j\sum_{k=i}\sum_{l=j} k_{tc,jl}Y_0^{ij}Y_0^{kl} + \sum_i\sum_j\sum_{k\neq i}\sum_{l\neq j} k_{tc,jl}Y_0^{ij}Y_0^{kl} + \sum_i\sum_j\sum_k\sum_l k_{td,jl}Y_0^{ij}Y_0^{kl} + k_{ct}[\left([P_0^{\bullet}] + \sum_i\sum_j Y_0^{ij}\right)\left(\sum_i\sum_j T_0^{ij} + \sum_i\sum_j\sum_k\sum_l X_0^{ij,kl}\right)$
First-order moments (i.e., molar conc. of monomer units in chains)	Propagating radical chains	$\frac{dY_1^{ij}}{dt} = 2k_{p,ij}[P_{1,i}^{\bullet}][M_j] + \sum_k k_{p,kij}[M_j]Y_0^{ki} + \sum_k k_{p,kij}[M_j]Y_1^{ki} - \sum_k k_{p,ijk}[M_k]Y_1^{ij} - 2\sum_{k=i=j} k_{p,ijk}[M_k]Y_0^{ij} - k_{a,j}Y_1^{ij}\left([TP_0] + \sum_k\sum_l Z_0^{kl}\right) + \frac{1}{2}k_{f,j}\left(T_1^{ij} + \sum_{k\neq i}\sum_{orl\neq l} X_{1,0}^{ij,kl} + \sum_{k=i}\sum_{l=j} X_1^{ij,kl}\right) - [k_{tc,ij}[P_0^{\bullet}] + \sum_k\sum_l \left(k_{tc,jl} + k_{td,jl}\right)Y_0^{kl}]Y_1^{ij} - k_{ct}Y_1^{ij}\left([P_0\dot{T}P_0] + \sum_k\sum_l T_0^{kl} + \sum_k\sum_l\sum_m\sum_n X_0^{kl,mn}\right)$
	Dormant chains	$\frac{dZ_1^{ij}}{dt} = \frac{1}{2}\left(k_{f,0}T_1^{ij} + \sum_{k\neq i}\sum_{orl\neq j} k_{f,l}X_{1,0}^{ij,kl} + \sum_{k=i}\sum_{l=j} k_{f,l}X_1^{ij,kl}\right) - \left(k_{a,0}[P_0^{\bullet}] + \sum_k\sum_l k_{a,l}Y_0^{kl}\right)Z_1^{ij}$
	Primary intermediate radical chains	$\frac{dT_1^{ij}}{dt} = k_{a,0}[P_0^{\bullet}]Z_1^{ij} + k_{a,j}[TP_0]Y_1^{ij} - \frac{1}{2}\left(k_{f,0} + k_{f,j}\right)T_1^{ij} - k_{ct}T_1^{ij}\left([P_0^{\bullet}] + \sum_k\sum_l Y_0^{kl}\right)$
	Intermediate radical chains	$\frac{dX_1^{ij,kl}}{dt} = k_{a,j}\left(Y_1^{ij}Z_0^{kl} + Y_0^{ij}Z_1^{kl}\right) - k_{f,j}X_1^{ij,kl} - k_{ct}X_1^{ij,kl}\left([P_0^{\bullet}] + \sum_m\sum_n Y_0^{mn}\right)\ (i=k, j=l)$
		$\frac{dX_1^{ij,kl}}{dt} = k_{a,j}\left(Y_1^{ij}Z_0^{kl} + Y_0^{ij}Z_1^{kl}\right) + k_{a,l}\left(Y_1^{kl}Z_0^{ij} + Y_0^{kl}Z_1^{ij}\right) - \frac{1}{2}\left(k_{f,j} + k_{f,l}\right)X_1^{ij,kl} - k_{ct}X_1^{ij,kl}\left([P_0^{\bullet}] + \sum_m\sum_n Y_0^{mn}\right)\ (i\neq k)\ \text{ or }\ (j\neq l)$
		$\frac{dX_{1,0}^{ij,kl}}{dt} = k_{a,j}Y_1^{ij}Z_0^{kl} + k_{a,l}Y_0^{ij}Z_1^{kl} - \frac{1}{2}\left(k_{f,j} + k_{f,l}\right)X_{1,0}^{ij,kl} - k_{ct}X_{1,0}^{ij,kl}\left([P_0^{\bullet}] + \sum_m\sum_n Y_0^{mn}\right)^a$
	Dead chains	$\frac{dQ_1}{dt} = (k_{tc,0} + k_{td,0})[P_0^{\bullet}]\sum_i\sum_j Y_1^{ij} + \sum_i\sum_j\sum_k\sum_l (k_{tc,jl} + k_{td,jl})Y_1^{ij}Y_0^{kl} + k_{ct}[\left([P_0^{\bullet}] + \sum_i\sum_j Y_0^{ij}\right)\left(\sum_i\sum_j T_1^{ij} + \sum_i\sum_j\sum_k\sum_l X_1^{ij,kl}\right) + k_{ct}\sum_i\sum_j Y_1^{ij}\left([P_0\dot{T}P_0]\sum_i\sum_j T_0^{ij} + \sum_i\sum_j\sum_k\sum_l X_0^{ij,kl}\right)$

Table 3. (*Continued*)

Second-order moments	Propagating radical chains	$\frac{dY_2^{ij}}{dt} = 4k_{p,ij}[P_{1,i}^{\bullet}][M_j] + \sum_k k_{p,kij}[M_j]Y_0^{kl} + 2\sum_k k_{p,kij}[M_j]Y_1^{ki} + \sum_k k_{p,kij}[M_j]Y_2^{ki} - \sum_k k_{p,ijk}[M_k]Y_2^{ij} - k_{a,j}Y_2^{ij}\left([TP_0] + \sum_k\sum_l Z_0^{kl}\right) + \frac{1}{2}k_{f,j}\left(T_2^{ij} + \sum_{k\neq i}\sum_{orl\neq l} X_{2,0}^{ij,kl} + \sum_{k=i}\sum_{l=j} X_2^{ij,kl}\right) - \{k_{tc,0}[P_0^{\bullet}] + \sum_k\sum_l (k_{tc,jl} + k_{td,jl})Y_0^{kl}\}Y_2^{ij} - k_{ct}Y_2^{ij}\left([P_0\dot{T}P_0] + \sum_k\sum_l T_0^{kl} + \sum_k\sum_l\sum_m\sum_n X_0^{kl,mn}\right)$
	Dormant chain	$\frac{dZ_2^{ij}}{dt} = \frac{1}{2}\left(k_{f,0}T_2^{ij} + \sum_k\sum_l k_{f,l}X_{2,0}^{ij,kl}\right) - (k_{a,0}[P_0^{\bullet}] + \sum_k\sum_l k_{a,l}Y_0^{kl}\right)Z_2^{ij}$
	Primary intermediate radical chains	$\frac{dT_2^{ij}}{dt} = k_{a,0}[P_0^{\bullet}]Z_2^{ij} + k_{a,j}[TP_0]Y_2^{ij} - \frac{1}{2}\left(k_{f,0} + k_{f,j}\right)T_2^{ij} - k_{ct}T_2^{ij}\left([P_0^{\bullet}] + \sum_k\sum_l Y_0^{kl}\right)$
	Intermediate radical chains	$\frac{dX_2^{ij,kl}}{dt} = k_{a,j}\left(Y_2^{ij}Z_0^{kl} + 2Y_1^{ij}Z_1^{kl} + Y_0^{ij}Z_2^{kl}\right) - k_{f,j}X_2^{ij,kl} - k_{ct}X_2^{ij,kl}\left([P_0^{\bullet}] + \sum_m\sum_n Y_0^{mn}\right)$ $(i = k, j = l)$ $\frac{dX_2^{ij,kl}}{dt} = k_{a,j}\left(Y_2^{ij}Z_0^{kl} + 2Y_1^{ij}Z_1^{kl} + Y_0^{ij}Z_2^{kl}\right) + k_{a,l}\left(Y_2^{kl}Z_0^{ij} + 2Y_1^{kl}Z_1^{ij} + Y_0^{kl}Z_2^{ij}\right) - \frac{1}{2}(k_{f,j} + k_{f,l})X_2^{ij,kl} - k_{ct}X_2^{ij,kl}\left([P_0^{\bullet}] + \sum_m\sum_n Y_0^{mn}\right)$ $(i \neq k)$ or $(j \neq l)$ $\frac{dX_{2,0}^{ij,kl}}{dt} = k_{a,j}Y_2^{ij}Z_0^{kl} + k_{a,l}Y_0^{ij}Z_2^{kl} - \frac{1}{2}(k_{f,j} + k_{f,l})X_{2,0}^{ij,kl} - k_{ct}X_{2,0}^{ij,kl}\left([P_0^{\bullet}] + \sum_m\sum_n Y_0^{mn}\right)^a$
	Dead chains	$\frac{dQ_2}{dt} = (k_{tc,0} + k_{td,0})[P_0^{\bullet}]\sum_i\sum_j Y_2^{ij} + \sum_i\sum_j\sum_k\sum_l k_{tc,jl}(Y_2^{ij}Y_0^{kl} + Y_1^{ij}Y_1^{kl}) + \sum_i\sum_j\sum_k\sum_l k_{td,jl}Y_2^{ij}Y_0^{kl} + k_{ct}[\left([P_0^{\bullet}] + \sum_i\sum_j Y_0^{ij}\right)\left(\sum_i\sum_j T_2^{ij} + \sum_i\sum_j\sum_k\sum_l X_2^{ij,kl}\right) + k_{ct}\sum_i\sum_j Y_2^{ij}\left([P_0\dot{T}P_0] + \sum_l\sum_j T_0^{ij} + \sum_i\sum_j\sum_k\sum_l X_0^{ij,kl}\right) + 2k_{ct}\sum_i\sum_j Y_1^{ij}\left(T_0^{ij} + \sum_i\sum_j\sum_k\sum_l X_1^{ij,kl}\right)$
Small molecules	Initiator	$\frac{d[I]}{dt} = -k_d[I]$
	Monomers	$\frac{d[M_i]}{dt} = -k_{in,i}[P_0^{\bullet}][M_i] - \sum_j k_{p,ji}[P_{1,j}^{\bullet}][M_i] - \sum_k\sum_j k_{p,kji}Y_0^{kj}[M_i]$

*These equations are necessary for closure of the differential equations.

Producing copolymers with a precisely controlled composition distribution along backbones provides a great challenge for polymer chemists and engineers. In our previous work,[23] we developed a kinetic model for the semibatch RAFT copolymerization. The work theoretically demonstrated the feasibility of designing and control of CCD in RAFT polymerization using semibatch feeding policies. This theoretical development was later extended to atom transfer radical copolymerization (ATRcoP).[24] In the experimental area, we demonstrated the first programmed synthesis of two simple types of copolymers (uniform and linear gradient copolymers) via semibatch RAFT copolymerization.[25] The former had a uniform composition distribution from one end to the other along backbone for all the individual polymer chains. The composition of the latter copolymer increased linearly from one end to the other. Smulders et al.[26] produced unique (multi)block copolymers of styrene and *n*-butyl acrylate by continuous RAFT miniemulsion polymerization.

In this work, we carried out a systematical experimental study on the preparation of copolymer products with various unprecedented chain microstructures through programmed semibatch RAFT copolymerization. We used styrene (1)/butyl acrylate (2) as a model system initiated by 1,1′-azobis (cyclohexane-carbonitrile) and mediated by benzyl dithioisobutyrate (BDIB). The microstructures included uniform, linear gradient, inverse linear gradient, hyperbolic tangent

Table 4. Diffusion-Controlled Termination Model and Semibatch Reactor Model

Diffusion-Controlled Termination Model	Semibatch Reactor Model
$v_f = [0.025 + \alpha_p(T - T_{gp})]\varphi_p + [0.025 + \alpha_{m1}(T - T_{gm1})]\varphi_{m1} + [0.025 + \alpha_{m2}(T - T_{gm2})]\varphi_{m2} + [0.025 + \alpha_s(T - T_{gs})]\varphi_s$ (1)*	$\frac{dV}{dt} = V_{s,in} + \sum_{i=1}^{2} F_{i,in} mw_{mi} \rho_{mi} - \sum_{i=1}^{2} R_{p,i} mw_{mi} \left(\frac{1}{\rho_{mi}} - \frac{1}{\rho_p}\right) V$ (4)
$k_{tii,D} = k^0_{tii,D} (\bar{r}_N)^{-a} \exp(-b/v_f)$ (2)**	$\frac{dV}{dt} = \frac{V_f \rho_f}{\rho} - \frac{V}{\rho}\frac{d\rho}{dt}$ (5)
$\frac{1}{k_{tii}} = \frac{1}{k_{tii,C}} + \frac{1}{k_{tii,D}} \quad (i = 1, 2)$ (3)†	$\frac{dC_i}{dt} = \frac{1}{V}\left(V_f C_{i,f} - C_i \frac{dV}{dt}\right) + R_i$ (6)

*Ref. 27
**Ref. 28
†Ref. 29–31.

(tanh) gradient, and triblock with a linear gradient mid-block profiles, as illustrated in Scheme 1. The experimental data of CC, polymerization rate, average molecular weight, and polydispersity were compared to their theoretically targeted values. In this work, we also evaluated, for the first time, the thermal properties of this novel series of copolymer samples and illustrated that the copolymers with different composition profiles have distinct thermal properties.

Theoretical Part

In our previous work,[25] we developed a detailed kinetic model for the semibatch RAFT copolymerization. The elementary reactions involved in the RAFT copolymerization, the definitions of various chain species and moments, the key mass balance equations, and the semibatch reactor model are briefly summarized in Tables 1–4, respectively.

Table 5 lists the values of all the kinetic rate constants employed in the simulation of the St/BA copolymerization system. Also listed in Table 5 are the values of all the physical and transport properties employed for the calculation of the diffusion-controlled terms.

The reactor model (Eqs. 4–6) together with the mass balance equations of various species in Table 3 form a complete set of equations for the semibatch RAFT copolymerization. Given appropriate initial conditions and values for the parameters, we can solve these ODE's numerically to obtain the average chain properties such as number–average chain length, weight–average chain length, polydispersity index, cumulative CC, as well as molar fraction of dead chains,

Table 5. Model Parameters

Parameter	Value	Parameter	Value
k_d (s^{-1})	$1.58 \times 10^{15} \exp(-15503/T)$ [32]	ρ_{m2} (g cm^{-3})	$0.9211 - 1 \times 10^{-3} (T - 273.15)$ [42]
k_{p11} (L mol^{-1} s^{-1})	$4.266 \times 10^7 \exp(-3909.61/T)$ [33]	ρ_p (g cm^{-3})	1.05 [42]
k_{p22} (L mol^{-1} s^{-1})	$7.37 \times 10^5 \exp(-1156.90/T)$ [34]	α_p (K^{-1})	$F_{n1}\alpha_{p1} + F_{n2}\alpha_{p2}$
k_{tc11} (L mol^{-1} s^{-1})	$1.91 \times 10^9 \exp(-958/T)$ [35]	α_{p1} (K^{-1})	4.5×10^{-4} [43]
k_{tc22} (L mol^{-1} s^{-1})	$2.57 \times 10^8 \exp(-672.35/T)$ [36]	α_{p2} (K^{-1})	4.8×10^{-4} [44]
k_{td11} (L mol^{-1} s^{-1})	0 [37]	α_{m1} (K^{-1})	1.0×10^{-3} [43]
k_{td22} (L mol^{-1} s^{-1})	0 [38]	α_{m2} (K^{-1})	1.19×10^{-3} [44]
k_{t12}, k_{t21} (L mol^{-1} s^{-1})	$(k_{t11} \cdot k_{t22})^{1/2}$ [39]	α_S (K^{-1})	1.215×10^{-3} [45]
r_1	0.956 [40]	T_{gm1} (K)	185.15 [35]
r_2	0.200 [40]	T_{gm2} (K)	185.15 [44]
s_1	1 [41]	T_{gS} (K)	115 [46]
s_2	0.012 [41]	T_{gp1} (K)	373 [43]
$k_{a,0}$ (M^{-1} s^{-1})	2.5×10^6*	T_{gp2} (K)	218 [44]
$k_{a,1}$ (M^{-1} s^{-1})	1×10^5*	T_{gp}	$(T_{gp1}\phi_1 + 0.85T_{gp2}\phi_2)/(\phi_1 + 0.85\phi_2)$ [47]
$k_{a,2}$ (M^{-1} s^{-1})	2.5×10^6*	$\langle k_{ct}\rangle / \langle k_t\rangle$**	0.04*
$k_{f,0}$ (s^{-1})	1×10^4*	$k^0_{t11,D}$	3.5×10^{12}†
$k_{f,1}$ (s^{-1})	1700*	$k^0_{t22,D}$	1×10^{12}†
$k_{f,2}$ (s^{-1})	1×10^4*	a	0.6†
ρ_{m1} (g cm^{-3})	$0.9193 - 6.65 \times 10^{-4} (T - 273.15)$ [42]	b	1.2†

*Obtained by our work.
**$\langle k_t \rangle = p_1^2 k_{t,11} + 2p_1 p_2 k_{t,12} + p_2^2 k_{t,22}$ where p_i is the relative concentration of terminal radical i.
†Obtained by experimental data fitting.

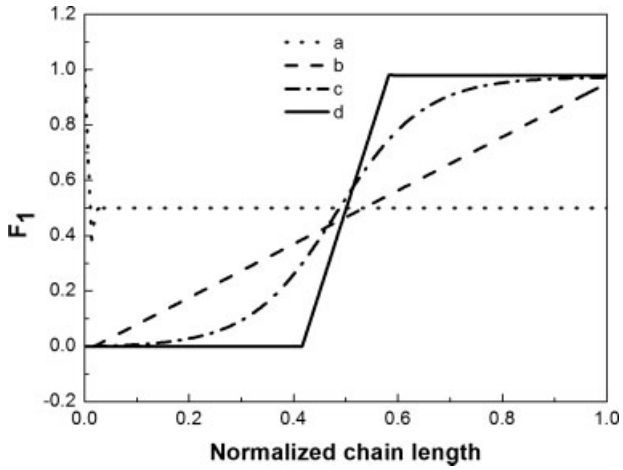

Figure 1. CCDs along chain backbone of the targeted copolymers: (a) uniform, (b) linear gradient, (c) hyperbolic tangent gradient, and (d) triblock copolymer.

$$\bar{r}_{\mathrm{N}} = \frac{\sum_i \sum_j \sum_k \sum_l (Y_1^{ij} + Z_1^{ij} + T_1^{ij} + X_1^{ij,kl} + Q_1)}{\sum_i \sum_j \sum_k \sum_l (Y_0^{ij} + Z_0^{ij} + T_0^{ij} + X_0^{ij,kl} + Q_0)} \tag{7a}$$

$$\bar{r}_{\mathrm{W}} = \frac{\sum_i \sum_j \sum_k \sum_l (Y_2^{ij} + Z_2^{ij} + T_2^{ij} + X_2^{ij,kl} + Q_2)}{\sum_i \sum_j \sum_k \sum_l (Y_1^{ij} + Z_1^{ij} + T_1^{ij} + X_1^{ij,kl} + Q_1)} \tag{7b}$$

$$\mathrm{PDI} = \frac{\bar{r}_{\mathrm{W}}}{\bar{r}_{\mathrm{N}}} \tag{7c}$$

$$F_{ni} = \frac{M_{i0} - M_{it} - M_{ir}}{\sum_{j=1}^{2} (M_{j0} - M_{jt} - M_{jr})} \tag{7d}$$

$$M_{\mathrm{n}} = \sum_{i=1}^{2} \bar{r}_{\mathrm{N}} F_{ni} m w_{mi} \tag{7e}$$

$$N_{\mathrm{dead}} = \frac{Q_0}{\sum_i \sum_j \sum_k \sum_l (Y_0^{ij} + Z_0^{ij} + T_0^{ij} + X_0^{ij,kl} + Q_0)} \tag{7f}$$

On the other hand, when a special composition profile is targeted, we can also solve ODE's to obtain the feeding rate vs. time profile by imposing a constraint equation,

$$F_1 = f(\bar{r}_{\mathrm{N}}) \tag{8}$$

where F_1 is CC, $\bar{r}_{\mathrm{N}}$ is number–average chain length. The form of function f can be designed according to the targeted composition profile. We designed four different composition profiles in this work: uniform, linear gradient (and inverse linear gradient), tanh gradient, and triblock with a linear gradient middle portion as transition block, as shown in Figure 1. The function f of these composition profiles are expressed as follows:

$$\text{Uniform:} \quad F_1 = \frac{R_{m1}}{R_{m1} + R_{m2}} = 0.5 \tag{9}$$

$$\text{Linear gradient:} \quad F_1 = \frac{\bar{r}_{\mathrm{N}}}{\bar{r}_{\mathrm{N,targeted}}} \tag{10}$$

$$\text{Tanh:} \quad F_1 = \frac{1}{2} + \frac{1}{2} \tanh\, \lambda \left(\frac{\bar{r}_{\mathrm{N}}}{\bar{r}_{\mathrm{N,targeted}}} - \frac{1}{2} \right), \quad (\lambda = 6 \text{ in this work}) \tag{11}$$

$$\text{Triblock:} \quad \begin{cases} F_1 = 0 & \bar{r}_{\mathrm{N}} \le \frac{5\bar{r}_{\mathrm{N,targeted}}}{12} \\ F_1 = \frac{6\bar{r}_{\mathrm{N}}}{\bar{r}_{\mathrm{N,targeted}}} - \frac{5}{2} & \frac{5\bar{r}_{\mathrm{N,targeted}}}{12} < \bar{r}_{\mathrm{N}} \le \frac{7\bar{r}_{\mathrm{N,targeted}}}{12} \\ F_1 = 1 & \bar{r}_{\mathrm{N}} > \frac{7\bar{r}_{\mathrm{N,targeted}}}{12} \end{cases} \tag{12}$$

By including the corresponding composition equation in the model, we can obtain a curve of feeding rate vs. time for a specifically targeted microstructure. The programming chart is illustrated in Scheme 2.

Experimental

Materials

Styrene (Shanghai Ling Feng Chemical Reagent, 99%) and BA (Shanghai Chemical Reagent, 98%) were purified by vacuum distillation. 1,1′-Azobis (cyclohexane-carbonitrile) (ACC, Aldrich, 98%) was purified by recrystallization from methanol. Toluene (Hangzhou Chemical Reagent, 99.5%) was used without purification. BDIB was synthesized following a procedure previously reported.[25] All the other chemicals were commercially obtained and used without purification.

Batch solution copolymerization

The batch RAFT solution polymerizations of St/BA were conducted at 88°C in 70 wt % toluene solutions (Run 1 in Table 6). The batch polymerizations were designed to investigate the influence of monomer composition on the polymerization kinetics. By fitting the kinetic models to the experimental data, the adjustable parameter for the diffusion-controlled termination ($k^0_{tii,D}$,a,b) in Table 5 could be obtained. In a typical run, the mixture of St, BA, toluene, ACC, and BDIB was transferred to several glass tubes of 7 mm diameter, followed by deoxygenation with pure nitrogen for five times. The sealed tubes were subsequently submerged in a water bath with the temperature controlled at 88°C. Each sealed tube was taken out at a preset time interval. The reaction was quenched by cooling the solution in an ice bath and a small amount of hydroquinone was added to stop the polymerization. The polymer materials were collected by evaporating the solvent and residual monomer. The final conversions were measured by gravimetry.

Semibatch solution copolymerization

A solution of St, BA, toluene (70 wt % monomers and 30 wt % toluene), and BDIB was initially charged to a

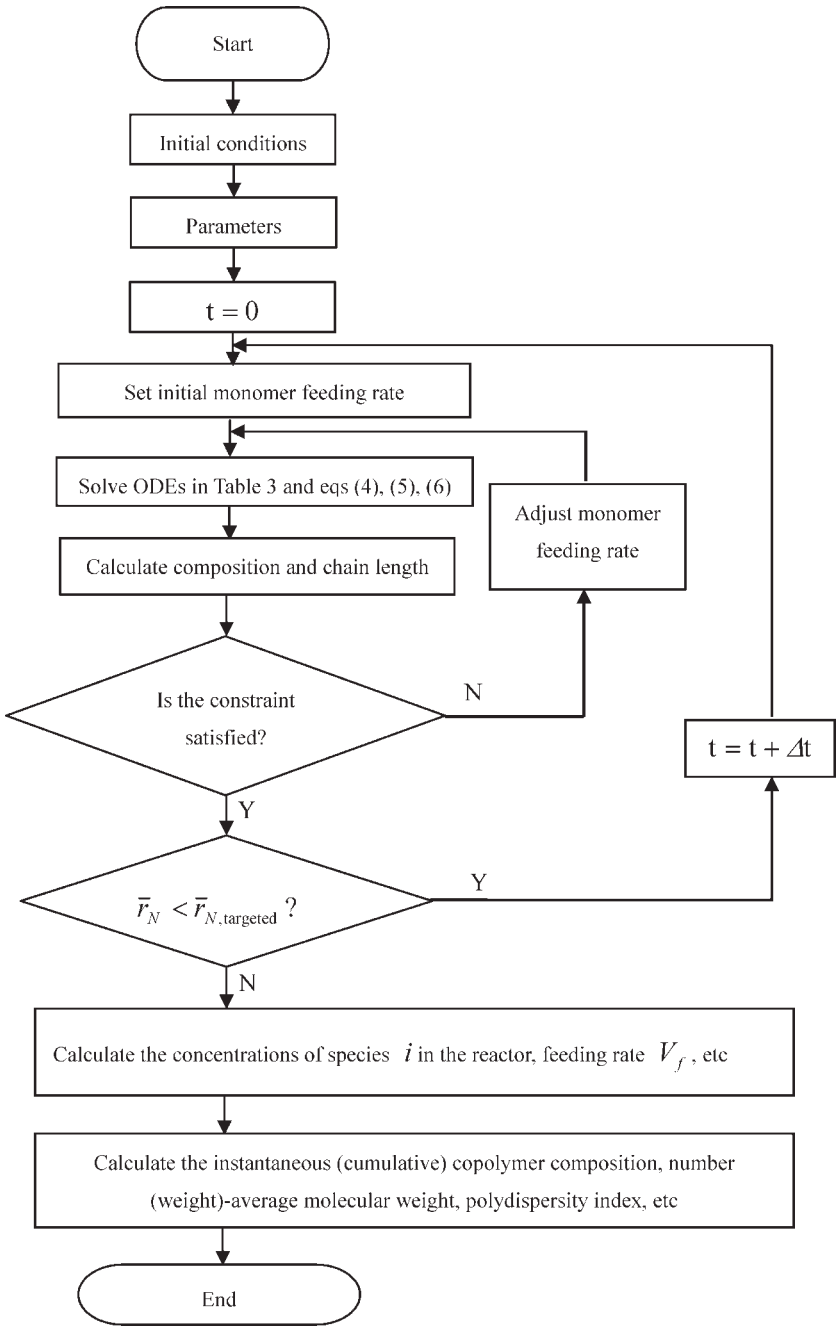

Scheme 2. Schematic calculation process.

500 mL five-neck flask, equipped with a condenser, a nitrogen inlet, a mechanical stirrer, and a syringe pump. The solution was stirred at room temperature for 20 min, and then immersed into a thermostated water bath at 88°C. The reactor was deoxygenated for 30 min before the solution was charged and was further deoxygenated by purging with nitrogen for 10 min at the water bath temperature. The addition of ACC in 5 g toluene set the zero time of the polymerization. The deoxygenized comonomer solution (70 wt % monomer in toluene) was continuously fed to the reactor according to a programmed feeding rate controlled by a metering pump connected to the computer. The samples were regularly withdrawn and quenched with hydroquinone.

Characterization of the polymer products

The average molecular weight and MWD of the copolymers were measured by gel permeation chromatography (GPC) on Waters 2487/630C with three Waters PL columns (10,000, 1000, and 500 Å) at 30°C. The eluent was tetrahydrofuran (THF) with a flow rate of 1 mL min^1. The resolution curve was calibrated using narrow PS standard samples with the molecular weight ranging from 580 to 710,000 g mol^{-1}.

Table 6. Recipes for all the Experimental Runs

Expt	St (g)	BA (g)	Initial St Molar Fraction, $f_{St,0}$	Amount of St(BA) Added in the Second Stage (g)*	Toluene (g)	ACC (g)	RAFT (g)
1a	19.60	0	1	–	8.40	0.0296	0.1184
1b	13.90	5.70	0.75	–	8.40	0.0280	0.1121
1c	8.79	10.81	0.5	–	8.40	0.0266	0.1064
1d	4.18	15.42	0.25	–	8.40	0.0253	0.1012
1e	1.63	17.97	0.1	–	8.40	0.0246	0.0983
1f	0	19.60	0	–	8.40	0.0241	0.0865
2	19.58	51.20	0.3197	38.09	30.33	0.1260	0.5040
3	0	51.20	0	95.63	21.94	0.1260	0.5040
4	41.66	0	1	78.26	17.85	0.1260	0.5040
5	0	51.20	0	110.57	21.94	0.1260	0.5040
6	0	51.20	0	121.88	21.94	0.1260	0.5040

*The recipe for semibatch copolymerization.

The cumulative polymer composition was determined by ^{1}H NMR spectroscopy (Bruker AC-80 spectrometer operated at 400 MHz). The analysis was carried out at room temperature in deuterated chloroform (~8% (W/V) solutions). The relative amounts of the comonomers incorporated in polymer chains were estimated from the areas under assigned peaks of the spectra. For St/BA copolymers, the peaks at approximately 6.5 ppm were assigned to the five protons on the benzene ring of St, while the peaks at approximately 3.5 ppm were assigned to the two protons of the methylene group close to the oxygen in the ester moiety of BA. The CC was determined by comparing the integrated intensities of these resonance signals.

The thermal analysis was carried out using a differential scanning calorimeter (DSC) of TA Instruments operated with TA Advantage Control software version 2.6D. Cooling was accomplished by a TA Instruments liquid nitrogen cooling accessory (LNCA). The dry nitrogen was purged into the DSC cell with a flow rate of 50 mL min^{-1}. The calorimeter was calibrated with an indium standard. The samples were annealed under vacuum for 36 h at 150°C to eliminate thermal history. Around 10 mg of sample was loaded into an aluminum pan with an empty pan serving as a reference. Each sample was cooled to 100°C at a rate of 40°C min^{-1}, and then heated to 150°C at a rate of 10°C min^{-1}.

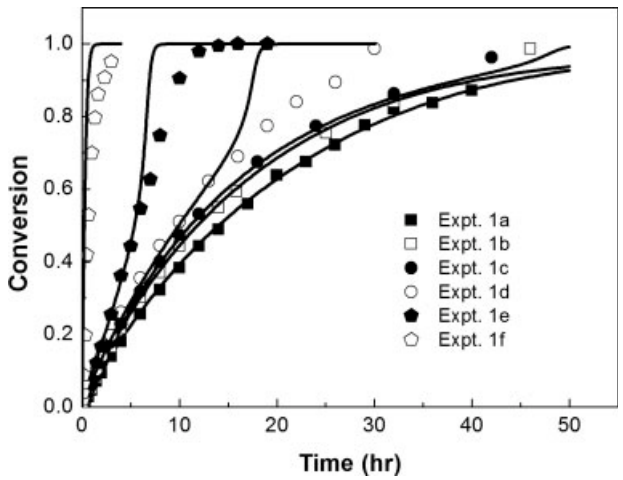

Figure 2. Comparison of model prediction and experimental data for the monomer conversion of St and BA with six different initial monomer ratios.

Polymerization temperature 88°C; $[monomer]_0$:$[BDIB]_0$:$[ACC]_0$ = 1000:3:0.645; solid content: 70%; initial monomer ratio (Expt. 1a, $f_{St,0}$ = 1; Expt. 1b, $f_{St,0}$ = 0.75; Expt. 1c, $f_{St,0}$ = 0.5; Expt. 1d, $f_{St,0}$ = 0.25; Expt. 1e, $f_{St,0}$ = 0.1; Expt. 1f, $f_{St,0}$ = 0). The points are experimental data while the lines are theoretical predictions.

Results and Discussion

Batch solution copolymerization of St and BA

The objective of this work is to demonstrate the use of the model-based computer-controlled semibatch RAFT copolymerization technology for preparing various copolymer products with carefully designed and precisely controlled composition profiles. The model serves as a predictive tool to first correlate conversion data for an estimate of some parameters. The model is then used to predict CC and to design the monomer feeding rate profile for a targeted composition distribution.

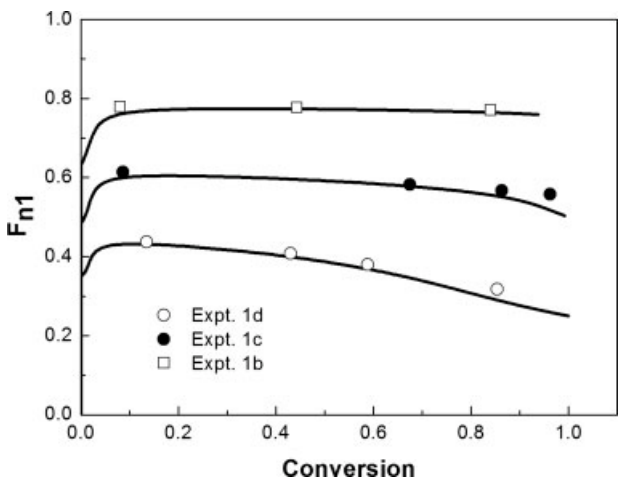

Figure 3. Comparison of model prediction and experimental data for the cumulative styrene CC vs. the total monomer conversion in the St/BA RAFT copolymerization at three different initial monomer ratios.

The experimental conditions are the same as in Figure 2.

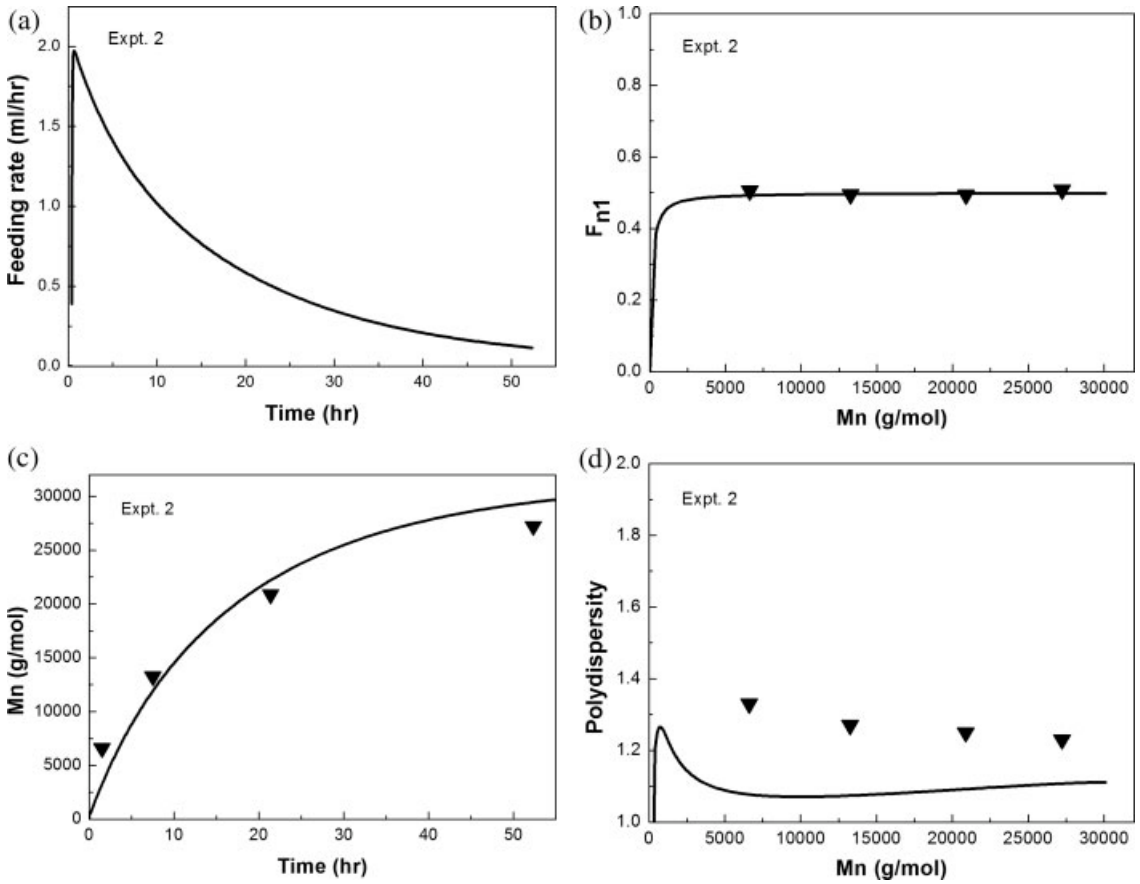

Figure 4. Semibatch St/BA RAFT copolymerization targeting for the uniform composition profile of $F_1 = 0.5$ (Expt. 2): (a) variation of volumetric feeding rate with time, (b) cumulative styrene CC vs. molecular weight, (c) molecular weight vs. reaction time, and (d) polydispersity vs. molecular weight.

Figure 2 shows the conversion histories at six levels of the initial St mole fraction ($f_{St,0}$). The solid curves are the theoretical results while the points are the experimental data. From this set of rate data, we estimated the diffusion-controlled termination parameter ($k^0_{tii,D}$,*a*,*b*), as given in Table 5. It is evident that the polymerization rate decreased with an increase of $f_{St,0}$. This is due to the higher value of BA propagation rate constant. The agreements between the theoretical and experimental values are good. The model was then employed for predicting the CC. Figure 3 gives the cumulative St mole fraction (F_{n1}) with respect to the total monomer conversion for three different $f_{St,0}$ levels. An excellent agreement exists between the model prediction and the experimental data. The model predicted that the cumulative styrene CC changed dramatically at low monomer conversions, which is different from the trend of conventional free radical polymerization (i.e. non-RAFT). It is attributed to the effect of RAFT process on the radical concentrations and to the selectivity of initiation reactions.[48]

St/BA copolymer with uniform composition

In most copolymerization systems, comonomers are consumed at different rates determined by the steric and electronic properties of reactants (i.e., monomer and radical species). Consequently, CC drifts with conversion in a batch process. Therefore, copolymers produced from a batch process generally do not have a uniform composition at a molecular level. In RAFT polymerization process, polymer chains grow slowly during the entire course of polymerization (in hours). This kinetic feature in chain growth yields copolymer chains with a gradient composition distribution along chain backbones from one end to the other. Through a semibatch process, RAFT copolymerization allows us to produce copolymers with well-controlled composition distribution profiles. In this section, we designed a copolymer with uniform chain composition at $F_1 = 0.5$ (Expt. 2). BA was charged to the reactor in the full amount at the very beginning of polymerization. St was partially charged to the reactor at the beginning. The amount of St initially charged to the reactor was calculated from Mayo-Lewis equation with the targeted CC ($F_1 = 0.5$), as seen in Table 6. As the polymerization proceeded, the rest amount of St was continuously fed to the reactor through a programmed metering pump. Incorporating Eq. 9 as the constraint condition into the model, we obtained the volumetric feeding rate vs. time curve through the model simulation as shown in Figure 4a.

Figure 4b shows the cumulative St mole fraction as a function of the number-average molecular weight with the programmed monomer feeding profile in Figure 4a. It is evident that the semibatch operation provided a good control over the drifting in CC (compared to Figure 3). It should be

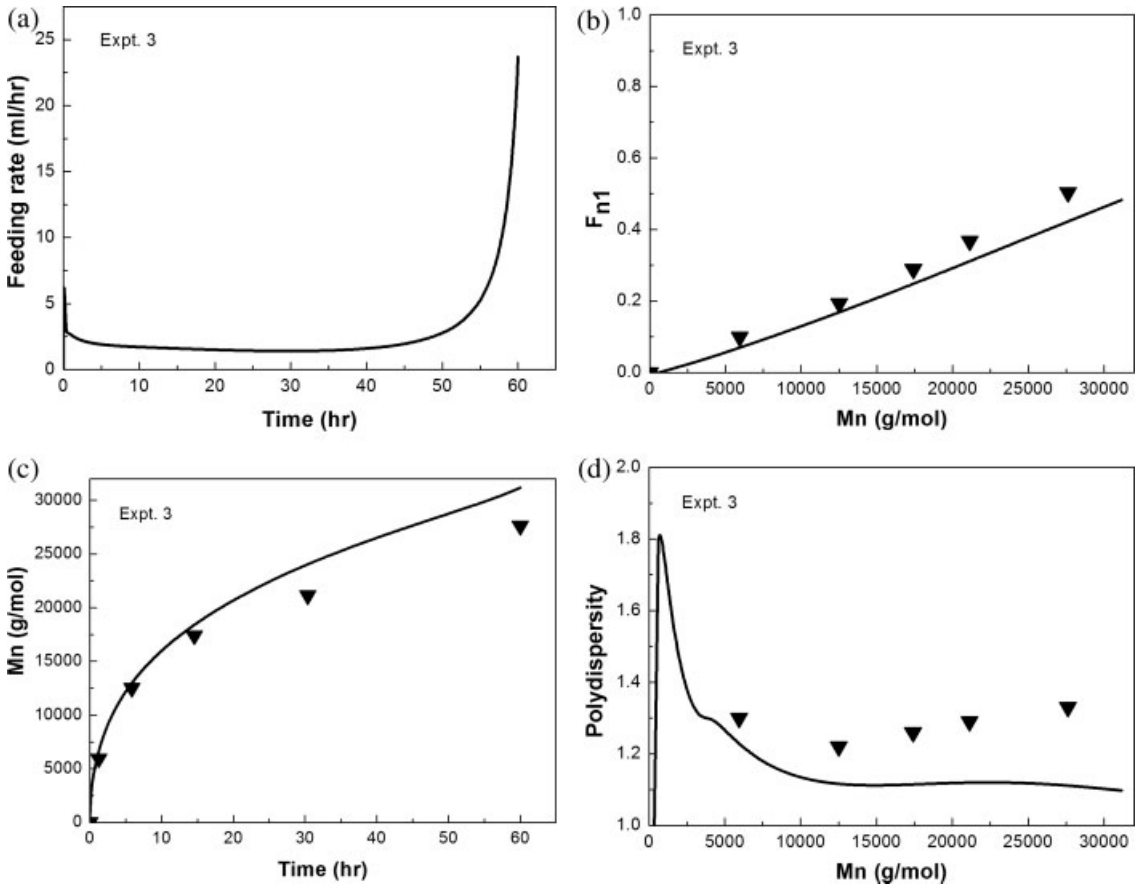

Figure 5. Semibatch St/BA RAFT copolymerization targeting for the linear gradient CC $F_1 = \bar{r}_N/\bar{r}_{N,targeted}$ (Expt. 3): (a) variation of volumetric feeding rate with time, (b) cumulative styrene CC vs. molecular weight, (c) molecular weight vs. reaction time, and (d) polydispersity vs. molecular weight.

pointed out that the control CC at the initial stage of polymerization was difficult because both radical concentration and CC changed dramatically. The feeding of St started after the RAFT system reached its steady state. As a result, the composition approached to the targeted value after the chains grew to 6 or 7 monomer units. Figure 4c shows the development of the molecular weight during the polymerization. The model successfully predicted the variation of molecular weight with reaction time. Figure 4d shows the trend of polydispersity and compares the experimental data to the simulated results. The experimental PDI values are less than 1.3 in a long period of the polymerization; however, the simulated values data are significantly lower than the experimental data. The deviation might be caused by branching reaction involving in the BA polymerization, which was not considered in the current model.

St/BA gradient copolymers with linear and tanh gradient compositions

Gradient copolymers have unique physical properties compared to traditional block or random copolymers of similar composition. However, preparation of gradient copolymers with controlled composition profile is challenging. In this section, we produced two representative symmetrical gradient copolymers: linear and tanh. For the linear gradient copolymer with $F_{n1} = 0.5$, using Eq. 10 as the constraint condition, we obtained the feeding rate vs. time profile as shown in Figure 5a. BA was initially charged to the reactor and St was fed by the programmed metering pump. The cumulative St mole fraction increased linearly from 0 to 0.5 as the chains grew (see Figure 5b). That is, the instantaneous CC of St increased linearly from 0 to 1, as Line b in Figure 1. Figure 5c shows the development of molecular weight with time and Figure 5d shows the polydispersity. It is evident in Figures 5b,c that the model predictions are in a good agreement with the experimental data. In Figure 5d, the model captures the trend. However, the experimental PDI data deviate from the model prediction, in particular, at high molecular weight (i.e. high conversion). This can also be explained by polymer branching reactions that involve BA units.

For this symmetrical linear gradient copolymer, we can also change the direction of polymer chain growth by initially charging the total amount of St to the reactor and feeding BA by the metering pump (an inverse mode of operation). In this case, the constraint condition should be as follows:

$$F_1 = 1 - \frac{\bar{r}_N}{\bar{r}_{N,targeted}} \tag{13}$$

The model results and experimental data are given in Figures 6a–d. It is of interest to see the complexity of the feed-

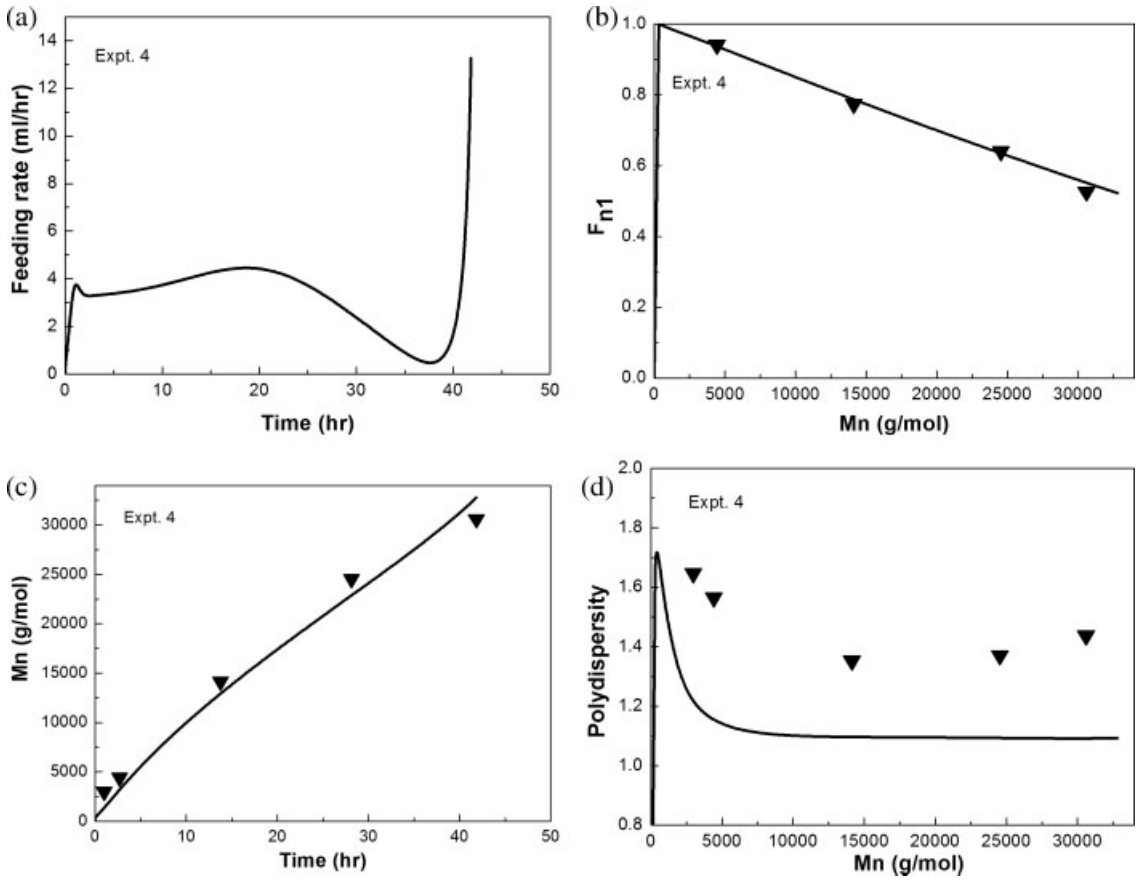

Figure 6. Semibatch St/BA RAFT copolymerzation targeting for the inverse linear gradient CC $F_1 = 1 - \bar{r}_N/\bar{r}_{N,\text{targeted}}$ (Expt. 4): (a) variation of volumetric feeding rate with time, (b) cumulative styrene CC vs. molecular weight, (c) molecular weight vs. reaction time, and (d) polydispersity vs. molecular weight.

ing rate vs. time curve. There is a compositional azeotropic point in the copolymerization of St/BA at about $f_{St} = 0.948$. When f_{St} is higher than 0.948, BA consumes faster than St does. When f_{St} is lower than 0.948, St consumes faster. Therefore, in the early of stage of polymerization, where BA consumed faster, the BA feeding rate needed to increase to meet the composition constraint. When the system passed the azeotropic point, St consumed faster than BA. When f_{St} in the system was lower than the value required by the constraint equation, the BA feeding rate decreased. When F_1 approached 0, f_{BA} in the reactor needed to be dramatically increased by a large amount of BA being charged to the reactor within a short period of time. In comparison of the two modes of operation, it took about 42 h in the inverse mode while it required 60 h in the normal mode to achieve the same targeted M_n and CC profile. The inverse mode is clearly advantageous over the normal mode in the polymerization rate. We compared the copolymers prepared by two modes in terms of NMR, GPC, and DSC data, respectively. The observed results are listed in Table 7. It can be concluded that these copolymers have similar structures.

Table 7. Summary of F_{n1}, M_n, and Glass Transition Temperature Data for the Linear Gradient Copolymers Produced in the Two Modes of Operation

Sample	F_{n1}	M_n (g mol^{-1})	T_0* (°C)	T_e* (°C)	ΔT_g (°C)
Normal	0.50	27,616	−36	37	73
Inverse	0.52	30,594	−39	34	73

*T_0 and T_e are the starting and ending points of the glass transition range, respectively.

For the tanh gradient copolymer, Eq. 11 was applied to obtain the feeding rate profile that is shown in Figure 7a. There was a maximal value in the feeding rate at about 39 h. At this point, the comonomer composition reached the azeotrope. After this point, St consumed more slowly than BA. Figure 7b shows the cumulative St CC profile (corresponding to the profile in Figure 1c). Figures 7c,d show the development of molecular weight and polydispersity, respectively. There is a fair agreement between the model prediction and experimental data. Some deviations in the agreement with composition and molecular weight are likely due to experimental errors.

St/BA triblock copolymer

Besides the uniform and gradient composition profiles, we also produced triblock copolymers with a linear gradient mid-block (refer to the profile (d) in Figure 1). Equation 12 was used as the constraint condition in calculating the monomer feeding policy. The triblock chain structure was accom-

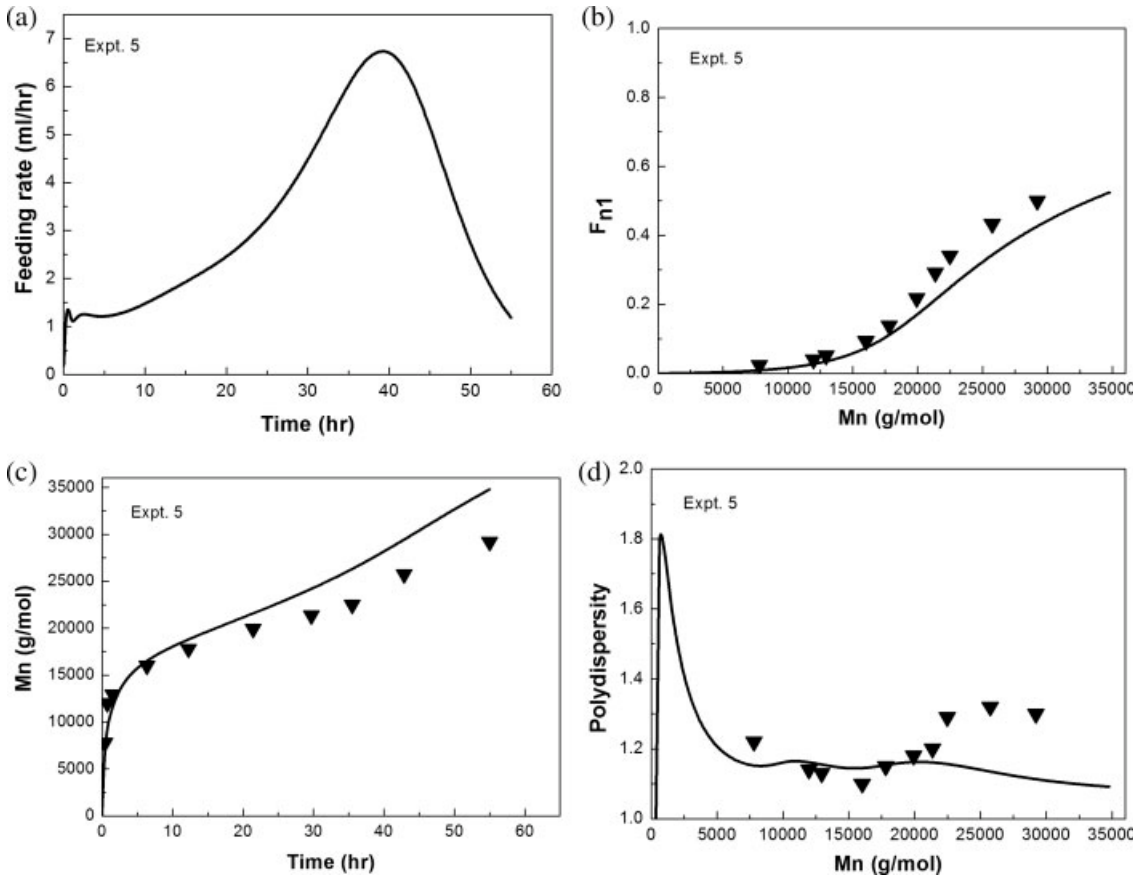

Figure 7. Semibatch St/BA RAFT copolymerization targeting for the hyperbolic tangent gradient CC as described by Eq. 12 (Expt. 5): (a) variation of volumetric feeding rate with time, (b) cumulative styrene CC vs. molecular weight, (c) molecular weight vs. reaction time, and (d) polydispersity vs. molecular weight.

plished in three steps. First, the total amount of BA was charged to the reactor. When the targeted degree of polymerization of the first block was reached, St was fed to generate the linear gradient block through a programmed metering pump. Finally, the rest amount of St was charged to the reactor to produce the homopolymer block of St. The simulation results and experimental data are shown in Figures 8a–d. The experimental data followed the model prediction. Again, the deviation of PDI can be seen in the high molecular weight section because of possible branching reactions. It can be seen in Figure 8c that the polymerization rate to generate the linear gradient block was much lower than that to of the homopolymer blocks of BA and St. The reason is that the apparent propagation rate constant of the St/BA copolymerization was lower than the propagation rate constant of the BA homopolymerization, and that the monomer concentration in the second stage was lower than that in the third stage.

Another important chain microstructural property in the CLRP is the fraction of dead chains in product. This information was also provided in our simulation. The molar fraction of the dead chains N_{dead} is shown in Figure 9. It can be seen that during the semibatch copolymerization, the molar fractions of dead chains were about 10% in all the five different cases. The amount of dead chains varied a lot, even though the ratio of RAFT and initiator concentrations remained the same. The reason for this is a variation in the polymerization rate, noting that the amount of dead chains is determined by the amount of decomposed initiator instead of the total amount charged to the reactor.

Thermal properties of the resulting copolymers

The glass transition behaviors of the above gradient copolymers were studied by DSC. The DSC heating curves of the products are shown in Figure 10. It is intriguing that the copolymers with the different composition profiles exhibited very different thermal properties. The uniform gradient copolymer gave a single value of T_g and a very narrow range of transition temperature ($\Delta T_g \sim 10^{\circ}C$). In contrast, there were substantial differences in the temperature range with the linear and tanh gradient copolymers. It was nearly 65°C with the linear gradient copolymer and 100°C with the tanh gradient copolymer. As far as the triblock copolymer is concerned, we observed multiple glass transitions in a broad temperature range ($\Delta T_g \sim 140^{\circ}C$) that extended from the T_g of polystyrene to that of poly(butyl acrylate). The broad range of transition indicates that there existed various time scales in chain relaxation, which can be attributed to the nano-heterogeneity of the materials.[49] Such materials have potential applications in sound and vibration damping. This preliminary DSC study clearly shows that the thermal proper-

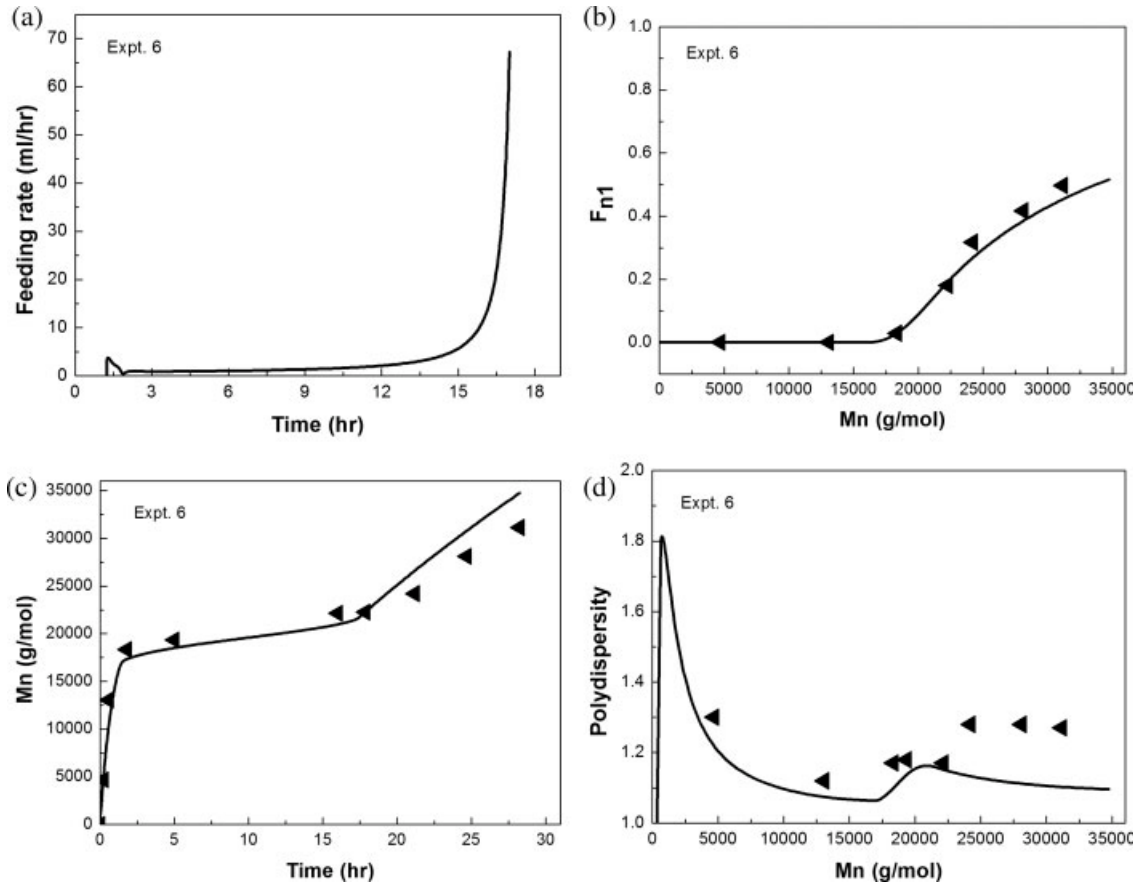

Figure 8. Semibatch St/BA RAFT copolymerzation targeting for the triblock copolymer as described by Eq. 13 (Expt. 6): (a) variation of volumetric feeding rate with time, (b) cumulative styrene CC vs. molecular weight, (c) molecular weight vs. reaction time, and (d) polydispersity vs. molecular weight.

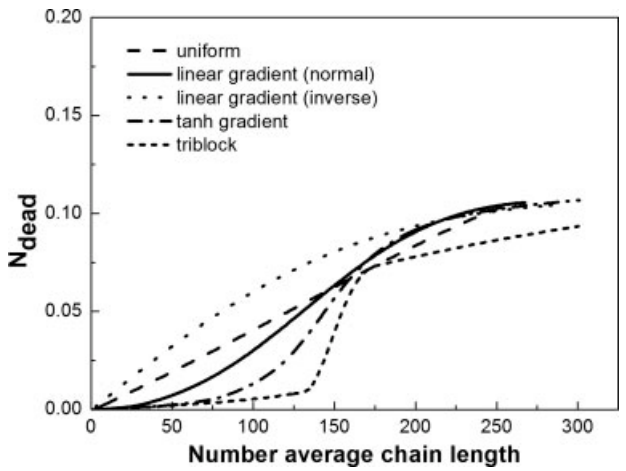

Figure 9. Molar fractions of dead chains vs. number–average chain length in the semibatch St/BA RAFT copolymerization that targets for uniform, linear gradient, tanh gradient, and triblock composition distributions.

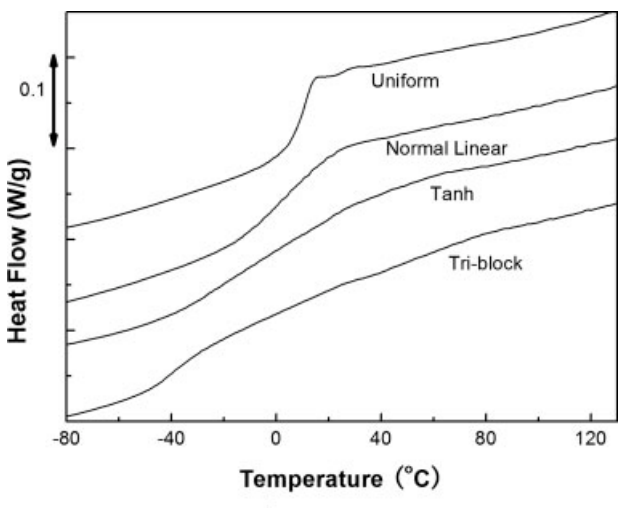

Figure 10. DSC heating curves for St/BA copolymers with uniform, linear gradient, tanh gradient and triblock composition distributions.

ties of gradient copolymer can be controlled by designing composition profiles with the semibatch strategy developed in this work.

Conclusions

In this work, we applied the developed semibatch RAFT copolymerization technology for the design and control of various gradient copolymers with unprecedented composition profiles. Using the technology, we produced a series of novel St/BA copolymers with uniform, linear gradient, tanh gradient, and triblock with a linear gradient mid-block composition profiles. The RAFT process proceeded in a living manner. The molecular weight data agreed with the model predictions. The MWDs were narrow with polydispersities about 1.3. The amount of dead chains was controlled below 10%. The experimental CCs followed the targeted profiles. This work demonstrated the usefulness of the model-based polymerization reactor technology in producing polymer materials with tailor-made chain microstructural properties. With this technology, we can design and prepare copolymer products with any gradient composition profile at will. We also carried out a preliminary study on the thermal properties of this novel series of copolymer products. It was found that the gradient profile has a significant effect on the glass transition behavior. The range of transition temperature increased in the order of uniform, linear gradient, tanh gradient, and triblock from 10°C for uniform to 140°C for triblock. This difference in the glass transition behavior reflected different morphologies that are determined by chain microstructural properties.

Acknowledgments

The authors would like to thank the National Science Foundation of China (#20774087, #20204015, JB), the Ministry of Education of China (Changjiang Scholar Visiting Fellowship, New Century Excellent Talent in University), and Zhejiang University for supporting this research program.

Notation

a = adjustable parameter for diffusion-controlled termination
b = adjustable parameter for diffusion-controlled termination
C_i = concentration of species i in reactor, mol L^{-1}
$C_{i,f}$ = concentration of species i in feed, mol L^{-1}
f_{BA} = BA mole fraction
f_{St} = St mole fraction
$f_{St,0}$ = initial St mole fraction
F_i = instantaneous copolymer composition of monomer i
$F_{i,in}$ = molar flow rate of monomer i into the reactor, mol s^{-1}
F_{ni} = cumulative copolymer composition of monomer i
k_a = addition rate coefficients, L mol^{-1} s^{-1}
k_{ct} = cross-termination between propagating and intermediate radicals, L mol^{-1} s^{-1}
k_d = Initiator decomposition rate constant, s^{-1}
k_f = fragmentation rate coefficient, s^{-1}
k_p = propagation rate constant, L mol^{-1} s^{-1}
k_t = termination reaction rate constant, L mol^{-1} s^{-1}
$<k_t>$ = apparent termination rate constant for copolymerization, L mol^{-1} s^{-1}
k_{tc} = termination by combination rate constant, L mol^{-1} s^{-1}
$k_{t,C}$ = chemical activation termination rate constant, L mol^{-1} s^{-1}
k_{td} = termination by disproportionation rate constant, L mol^{-1} s^{1}
$k_{t,D}$ = diffusion-controlled termination rate constant, L mol^{-1} s^{1}
$k^0_{t,D}$ = adjustable parameter for diffusion-controlled termination
mw_{mi} = molecular weight of monomer i, g mol^{-1}
M_{i0} = total mole of monomer i
M_{ir} = mole of monomer i in the reactor
M_{it} = mole of monomer i in the tank
M_n = number-average molecular weight, g mol^{-1}
N_{dead} = mole fraction of dead chains
p_i = relative concentration of terminal radical i
$P^{\bullet}_0$ = primary radical
PDI = polydispersity index
P_r = dead chain with length r
$P^{\bullet}_{r,ij}$ = propagating radical with chain length r, i-type penultimate unit and j-type terminal unit
$P_{r,ij}\dot{T}P_0$ = primary intermediate radical chain with chain length r, i-type penultimate unit, and j-type terminal unit
$P_{r,ij}\dot{T}P_{s,kl}$ = intermediate radical that have two "arms" with chain lengths r and s, adjacent penultimate units i and k, adjacent terminal units j and l
Q_m = moment of dead polymer chain
r_i = reactivity ratio for monomer i
R_i = reaction rate of species i, mol L^{-1} s^{-1}
$R_{p,i}$ = intrinsic propagation rate of monomer i, mol L^{-1} s^{-1}
$\bar{r}_N$ = number-average chain length
$\bar{r}_W$ = weight-average chain length
S_i = radical reactivity ratio for monomer i
T = temperature, K
T_g = glass-transition temperature, K
T^{ij}_m = moment of primary intermediate radical chain
TP_0 = RAFT agent
$TP_{r,ij}$ = dormant chain with chain length r, i-type penultimate unit, and j-type terminal unit
V = reactor volume, L
V_f = volumetric feeding rate, L s^{-1}
$V_{s,in}$ = volumetric flow rate of solvent into the reactor, L s^{-1}
$X^{ij,kl}_m$ = moment of intermediate radical chain
Y^{ij}_m = moment of propagating radical chain
Z^{ij}_m = moment of dormant chain

Greek letters

α = thermal expansion coefficient, K^{-1}
φ = volume fraction
v_f = free volume fraction, cm^3 g^{-1}
ρ = density of reaction mixture, g cm^{-3}
ρ_i = density of component i, g cm^{-3}
ρ_f = density of feeding materials, g cm^{-3}

Subscripts

m_i = monomer i
p = polymer
S = solvent
1 = St
2 = BA

Literature Cited

1. Matyjaszewski K, Xia JH. Atom transfer radical polymerization. *Chem Rev*. 2001;101:2921–2990.
2. Moad G, Rizzardo E, Thang SH. Living radical polymerization by the RAFT process. *Aust J Chem*. 2005;58:379–410.
3. Goto A, Fukuda T. Kinetics of living radical polymerization. *Prog Polym Sci*. 2004;29:329–385.
4. Georges MK, Veregin RPN, Kazmaier PM, Hamer GK. Narrow molecular weight resins by a free-radical polymerization process. *Macromolecules*. 1993;26:2987–2988.
5. Hawker CJ. Molecular weight control by living free radical polymerization process. *J Am Chem Soc*. 1994;116:11185–11186.
6. Moad G, Rizzardo E, Solomon DH. Selectivity of the reaction of free radicals with styrene. *Macromolecules*. 1982;15:909–914.
7. Matyjaszewski K, Gaynor S, Wang JS. Controlled radical polymerizations: the use of alkyl iodides in degenerative transfer. *Macromolecules*. 1995;28:2093–2095.

8. Fukuda T, Goto A, Ohno K. Mechanisms and kinetics of living radical polymerizations. *Macromol Rapid Commun*. 2000;21:151–165.
9. Faucher S, Okrutny P, Zhu S. Facile and effective purification of polymers produced by atom transfer radical polymerization via simple catalyst precipitation and microfiltration. *Macromolecules*. 2006; 39:3–5.
10. Chiefari J, Chong YK, Ercole F, Krstina J, Jeffery J, Le TPT, Mayadunne RTA, Meijs GF, Moad CL, Moad G, Rizzardo E, Thang SH. Living free-radical polymerization by reversible addition-fragmentation chain transfer: the RAFT process. *Macromolecules*. 1998;31: 5559–5562.
11. Barner-Kowollik C, Buback M, Charleux B, Coote ML, Drache M, Fukuda T, Goto A, Klumperman B, Lowe AB, Mcleary JB, Moad G, Monteiro MJ, Sanderson RD, Tonge MP, Vana P. Mechanism and kinetics of dithiobenzoate-mediated RAFT polymerization. I. The current situation. *J Polym Sci Part A: Polym Chem*. 2006;44: 5809–5831.
12. Luo Y, Wang R, Yang L, Yu B, Li B, Zhu S. Effect of reversible addition-fragmentation transfer (RAFT) reactions on (mini)emulsion polymerization kinetics and estimate of RAFT equilibrium constant. *Macromolecules*. 2006;39:1328–1337.
13. Quemener D, Davis TP, Barner-Kowollik C, Stenzel MH. RAFT and click chemistry: a versatile approach to well-defined block copolymers. *Chem Commun*. 2006;48:5051–5053.
14. Britze A, Moosmann K, Jahne E, Adler HJ, Kuckling D. Synthesis of block copolymers modified with phosphonate ester groups using nitroxide-mediated radical polymerizationa. *Macromol Rapid Commun*. 2006;27:1906–1912.
15. Miura Y, Okada M. Synthesis of graft copolymer by ATRP of MMA from poly(phenylacetylene). *J Polym Sci Part A: Polym Chem*. 2006;44:6697–6707.
16. Tsujii Y, Ohno K, Yamamoto S, Goto A, Fukuda T. Structure and properties of high-density polymer brushes prepared by surface-initiated living radical polymerization. *Adv Polym Sci*. 2006;197:1–45.
17. Gao HF, Matyjaszewski K. Structural control in ATRP synthesis of star polymers using the arm-first method. *Macromolecules*. 2006;39: 3154–3160.
18. Matyjaszewski K, Ziegler MJ, Arehart SV, Greszta D, Pakula T. Gradient copolymers by atom transfer radical copolymerization. *J Phys Org Chem*. 2000;13:775–786.
19. Avehart SV, Matyjaszewski K. Atom transfer radical copolymerization of styrene and *n*-butyl acrylate. *Macromolecules*. 1999;32:2221–2231.
20. Davis KA, Matyjaszewski K. Statistical, gradient, block, and graft copolymers by controlled/living radical polymerizations. *Adv Polym Sci*. 2002;159:1–166.
21. Min K, Li M, Matyjaszewski K. Preparation of gradient copolymers via ATRP using a simultaneous reverse and normal initiation process. I. Spontaneous gradient. *J Polym Sci Part A: Polym Chem*. 2005;43: 3616–3622.
22. Ziegler MJ, Matyjaszewski K. Atom transfer radical copolymerization of methyl methacrylate and *n*-butyl acrylate. *Macromolecules*. 2001;34:415–424.
23. (a) Wang R, Luo Y, Li BG, Sun X, Zhu S. Design and control of copolymer composition distribution in living radical polymerization using semi-batch feeding policies: a model simulation. *Macromol Theory Simul*. 2006;15:356–368.
24. Wang R, Luo Y, Li BG, Zhu S. Control of gradient copolymer composition in ATRP using semibatch feeding policy. *AICHE J*. 2007; 53:174–186.
25. Sun X, Luo Y, Wang R, Li BG, Liu B, Zhu S. Programmed synthesis of copolymer with controlled chain composition distribution via semibatch RAFT copolymerization. *Macromolecules*. 2007;40:849–859.
26. Smulders WW, Jones CW, Schork FJ. Synthesis of block copolymers using RAFT. Miniemulsion polymerization in a train of CSTRs. *Macromolecules*. 2004;37:9345–9354.
27. Achilias DS, Kiparissides C. Modeling of diffusion-controlled free-radical polymerization reactions. *J Appl Polym Sci*. 1988;35:1303–1323.
28. Marten FL, Hamielec AE. High-conversion diffusion-controlled polymerization of styrene. *J Appl Polym Sci*. 1982;27:489–505.
29. Gilbert RG. *Emulsion Polymerization: A Mechanistic Approach*; London: Academic, 1995.
30. Wang AR, Zhu S. Effects of diffusion-controlled radical reactions on RAFT polymerization. *Macromol Theory Simul*. 2003;12:196–208.
31. Noyes RM. In: Porter G, editor. *Effects of Diffusion Rates on Chemical Kinetics*. London: Pergamon, 1961.
32. Brandrup J, Immergut E, Grulke E, editors. *Polymer Handbook*, *4th ed*. New York: Wiley, 1999.
33. Buback M, Gilbert RG, Hutchinson RA, Klumperman B, Kuchta F, Manders BG, O'Driscoll KF, Russell GT, Schweer J. Critically evaluated rate coefficients for free-radical polymerization. I. Propagation rate coefficient for styrene. *Macromol Chem Phys*. 1995;196:3267–3280.
34. Beuermann S, Paquet DA Jr, McMinn JH, Hutchinson RA. Determination of free-radical propagation rate coefficients of butyl, 2-ethylhexyl, and dodecyl acrylates by pulsed-laser polymerization. *Macromolecules*. 1996;29:4206–4215.
35. Buback M, Kowollik C, Kurz C, Wahl A. Termination kinetics of styrene free-radical polymerization studied by time-resolved pulsed laser experiments. *Macromol Chem Phys*. 2000;201:464–469.
36. Li D, Grady MC, Hutchinson RA. High-temperature semibatch free radical copolymerization of butyl methacrylate and butyl acrylate. *Ind Eng Chem Res*. 2005;44:2506–2517.
37. Keramopoulos A, Kiparissides C. Development of a comprehensive model for diffusion-controlled free-radical copolymerization reactions. *Macromolecules*. 2002;35:4155–4166.
38. Keramopoulos A, Kiparissides C. Mathematical modeling of diffusion-controlled free-radical terpolymerization reactions. *J Appl Polym Sci*. 2003;88:161–176.
39. Walling C. Copolymerization. XIII. Over-all rates in copolymerization polar effects in chain initiation and termination. *J Am Chem Soc*. 1949;71:1930–1935.
40. Beuermann S, Buback M. Rate coefficients of free-radical polymerization deduced from pulsed laser experiments. *Prog Polym Sci*. 2002; 27:191–254.
41. Davis TP, O'Driscoll KF, Piton MC, Winnik MA. Copolymerization propagation kinetics of styrene with alkyl acrylates. *Polym Int*. 1991; 24:65–70.
42. Zhang M, Ray WH. Modeling of "living" free-radical polymerization processes. I. Batch, semibatch, and continuous tank reactors. *J Appl Polym Sci*. 2002;86:1630–1662.
43. Soh SK, Sundserg DC. Diffusion-controlled vinyl polymerization. III. Free volume parameters and diffusion-controlled propagation. *J Polym Sci Polym Chem Ed*. 1982;20:1331–1344.
44. Dube MA, Rilling K, Penlidis A. A kinetic investigation of butyl acrylate polymerization. *J Appl Polym Sci*. 1991;43:2137–2145.
45. Yao Y, Xie T, Gao Y, editors. *Handbook of Chemistry and Physics*. Shanghai: Shanghai Scientific and Technical Publishers, 1985.
46. Fedors RF. A universal reduced glass transition temperature for liquids. *J Polym Sci Polym Letters Ed* 1979;17:719–722.
47. Miwa Y, Usami K, Yamamoto K, Sakaguchi M, Sakai M, Shimada S. Direct detection of effective glass transitions in miscible polymer blends by temperature-modulated differential scanning calorimetry. *Macromolecules*. 2005;38:2355–2361.
48. Feldermann A, Toy AA, Phan H, Stenzel MH, Davis TP, Barner-Kowollik C. Reversible addition fragmentation chain transfer copolymerization: influence of the RAFT process on the copolymer composition. *Polymer*. 2004;45:3997–4007.
49. Lefebvre MD, Olvera de la Cruz M, Shull KR. Phase segregation in gradient copolymer melts. *Macromolecules*. 2004;37:1118–1123.

Manuscript received Jun. 13, 2007, and revision received Dec. 28, 2007.